CERES S-NPP Edition2A SSF

CERES shortwave (SW), longwave (LW), and window (WN) channel radiative fluxes are derived from empirical Angular Distribution Models (ADMs) that convert a measured radiance in a given Sun-Earth-satellite viewing configuration to a top-of-atmosphere (TOA) radiative flux. As there is no rotating azimuth scan mode for the flight model (FM5) on S-NPP, the ADMs developed for Aqua are used to convert the measured radiances to fluxes on S-NPP. Further details about the Aqua ADMs can be found in Su et al. (2015) and the table below provide additional details on Aqua ADM scene classification.

CERES Terra/Aqua Shortwave Channel ADMs for Different Scene Types

Scene Type	Description
Clear Ocean	Function of wind speed, aerosol optical depth, and aerosol type;
Cloud Ocean	Function of cloud phase; Continuous 5-parameter sigmoid function of cloud fraction and cloud optical depth.
Land & Desert Clear	1°- regional monthly ADMs using modified Ross-Li 3-parameter fit for difference NDVI, $\cos\theta_0$ and surface roughness (θ_0 is solar zenith angle);
Land & Desert Cloud	Function of cloud phase; continuous 5-parameter sigmoid function of cloud cover and cloud optical depth; used 1°-regional clear-sky BRDFs to account for background albedo.
Permanent Snow	Clear Antarctica: use MISR data to develop ADMs that account for the effect of sastrugi Clear Greenland: one ADM
	Partly cloudy: cloud fraction (4)
	Overcast: cloud phase (2), and log optical depth bin (4)
Fresh Snow	1°- regional monthly ADMs using modified Ross-Li 3-parameter fit for difference NDVI, $\cos\theta_0$ and surface roughness (θ_0 is solar zenith angle);
	Cloudy: function of cloud fraction and snow fraction; for overcast consider surface brightness and cloud optical depth
Sea-Ice	Clear: sea ice fraction (6), for 100% sea ice coverage use sea ice brightness index (3) to classify surface brightness
	Partly cloudy: cloud fraction (4), for 100% sea ice coverage use sea ice brightness index (3) to classify surface brightness
	Overcast: sea ice brightness index (5), phase (2), linear function of ln(cloud optical depth)

CERES Terra/Aqua Longwave and Window Channel ADMs for Different Scene Types

Scene Type	Description
Clear Ocean, Land, Desert	Function of Ocean, Forest, Cropland/Grass, Savanna, Bright Desert, Dark Desert, precipitable water, lapse rate, skin temperature.
Clouds Over Ocean, Land Desert	Function of precipitable water, skin temp, surface-cloud temp. diff; continuous function of parameterization involving cloud fraction, cloud and surface emissivity, surface and cloud temp.
Clear Permanent Snow, Fresh Snow, Sea-Ice	Discrete intervals of surface skin temperature.
Cloudy Permanent Snow, Fresh Snow, Sea-Ice	Function skin temp, surface-cloud temperature difference; continuous function of parameterization involving cloud fraction, cloud and surface emissivity, surface and cloud temp.

TOA Flux differences between S-NPP and Aqua

The Edition2A S-NPP radiances are on the same radiometric scales as Edition4A Aqua (Shankar et al. 2020). However, the slight difference between Aqua and S-NPP orbits leads to overpass time difference, thus the solar zenith angle distributions between them are different. Figure 1 shows the solar zenith angle as a function of latitude sampled by Aqua (left) and S-NPP (right) for April 2013. For a given latitude, S-NPP covers a wider range of solar zenith angle than Aqua. For April 2013, the solar zenith angles at the S-NPP overpass times are also smaller than the solar zenith angles at the Aqua overpass times, except over the north pole.

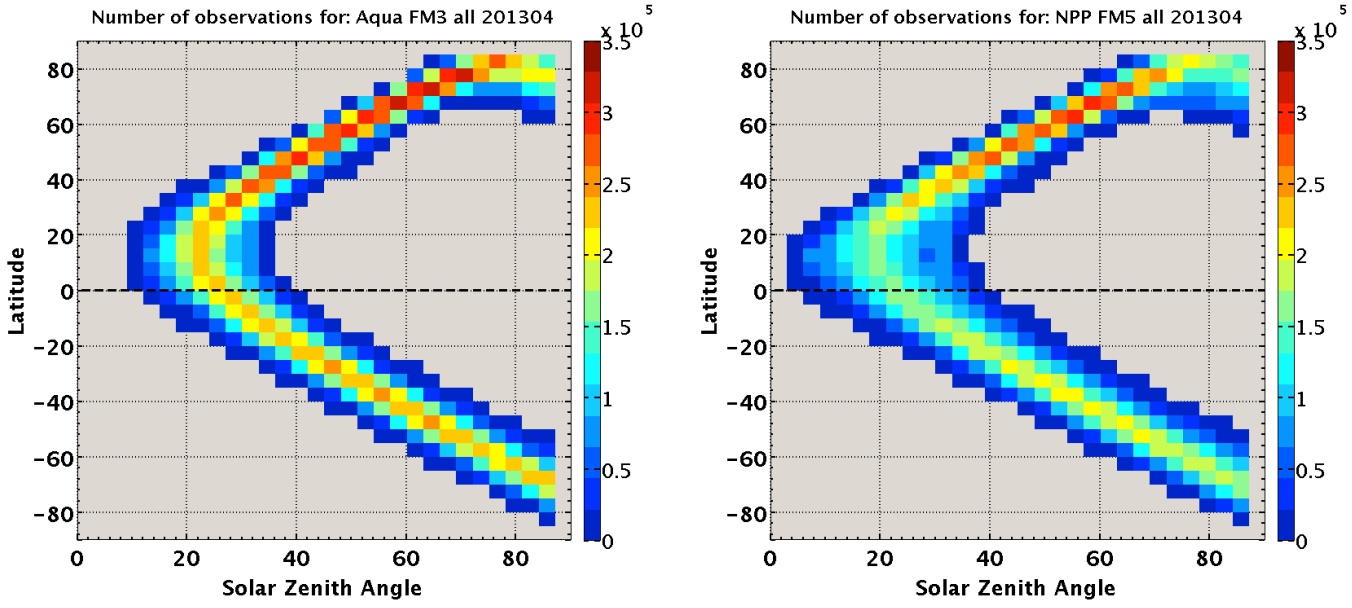

Figure 1. Solar zenith angle as a function of latitude sampled by Aqua (left) and S-NPP (right) for April 2013.

The solar zenith angle difference between S-NPP and Aqua results in that the monthly mean solar insolation from S-NPP is larger than that from Aqua by 13.4 Wm^{-2} (1.4%) for April 2013. Figure 2 shows the monthly mean TOA upwelling SW flux from S-NPP and the SW flux difference between S-NPP and Aqua for April 2013. The monthly mean TOA upwelling SW flux from S-NPP is about 1.1% higher than that from Aqua, and

some distinct features were observed (such as the large negative difference north of 60°N and the slant paths south of 60°S). These features are caused by the differences in solar insolation and disappeared in the albedo difference (Figure 3). The remaining difference between S-NPP and Aqua after accounting for the difference in solar insolation is about 0.7 Wm^{-2}.

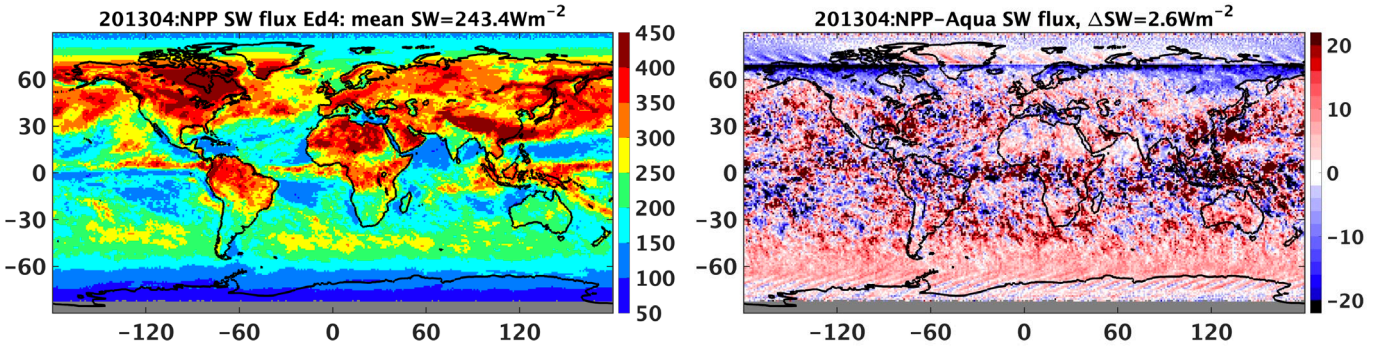

Figure 2. Monthly mean TOA upwelling SW flux from S-NPP (left) and the flux difference between S-NPP and Aqua (right) for April 2013.

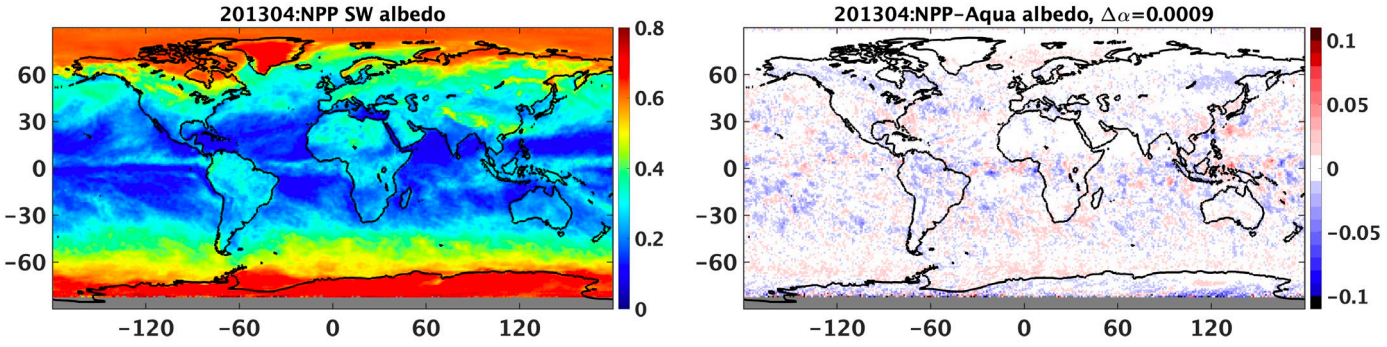

Figure 3. Monthly mean albedo from S-NPP (left) and the albedo difference between S-NPP and Aqua (right) for April 2013.

Figure 4 and Figure 5 show the monthly mean daytime and nighttime TOA outgoing LW flux from S-NPP and the difference between S-NPP and Aqua for April 2013. For both daytime and nighttime, the TOA outgoing LW flux from S-NPP is smaller than that from Aqua by less than 1 Wm-2.

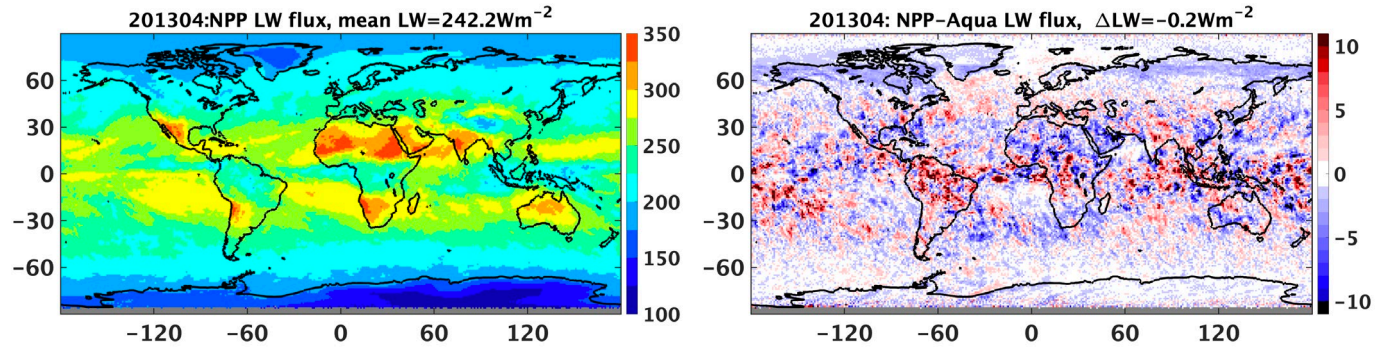

Figure 4. Monthly mean daytime TOA outgoing LW flux from S-NPP (left) and the difference between S-NPP and Aqua (right) for April 2013.

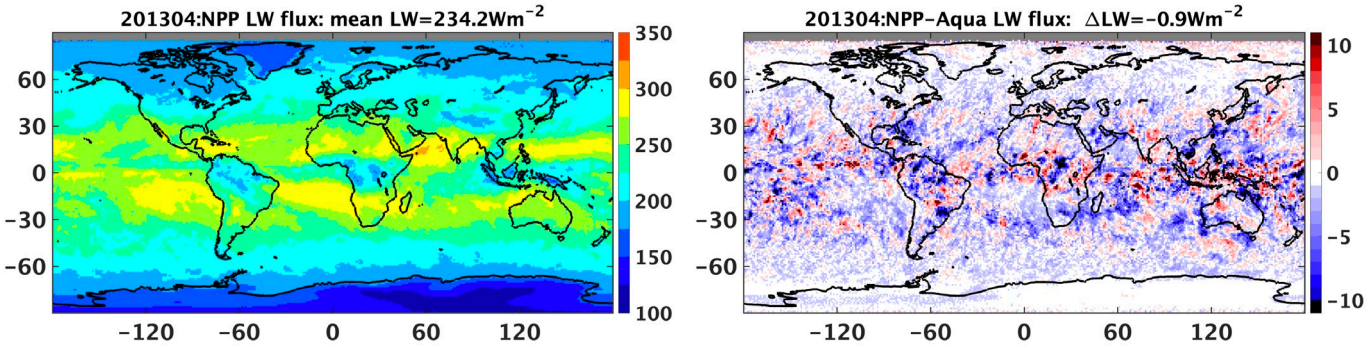

Figure 5. Monthly mean nighttime TOA outgoing LW flux from S-NPP (left) and the difference between S-NPP and Aqua (right) for April 2013.

The causes for the flux differences shown here are mainly due to 1) scene identification, as some MODIS channels used for cloud retrievals are not available on VIIRS; 2) use of the ADMs developed with Aqua measurements for S-NPP. Figure 6 and Figure 7 show the cloud fraction and cloud optical depth differences between S-NPP and Aqua for daytime and nighttime. These scene identification differences are currently being investigated by the CERES science team members and will be minimized in the future editions by incorporating CrIS observations and improving retrieval algorithms.

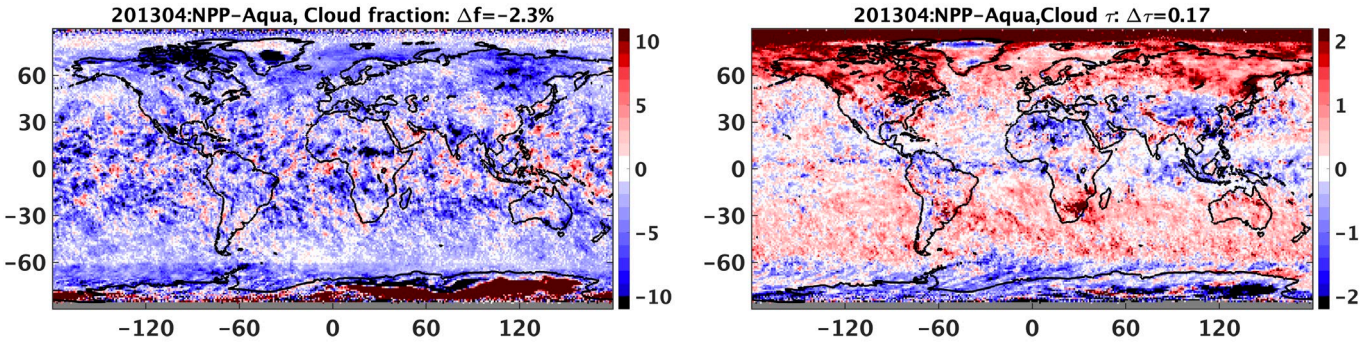

Figure 6. Monthly mean daytime cloud fraction difference (left) and cloud optical depth difference (right) between S-NPP and Aqua (right) for April 2013.

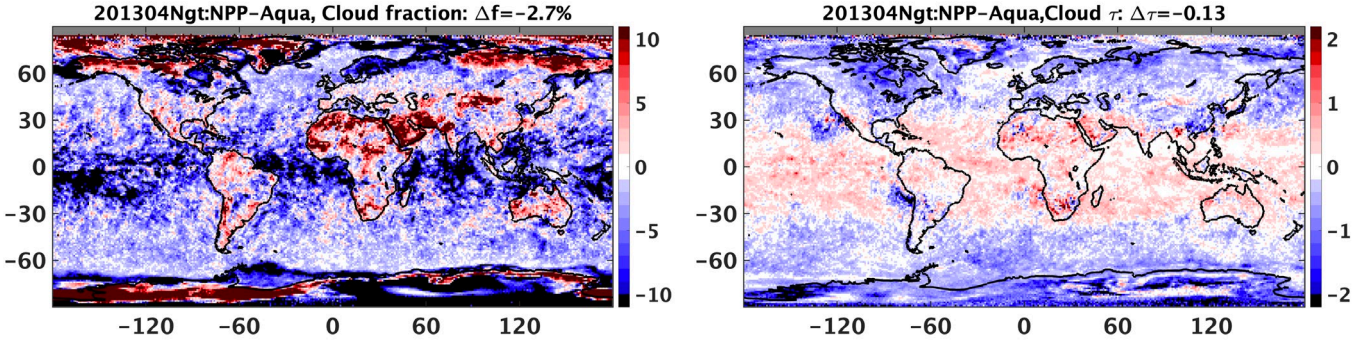

Figure 7. Monthly mean nighttime cloud fraction difference (left) and cloud optical depth difference (right) between S-NPP and Aqua (right) for April 2013.

References

Wenying Su, Joseph Corbett, Zachary Eitzen, Lusheng Liang, Next-Generation Angular Distribution Models for Top-of-Atmosphere Radiative Flux Calculation from the CERES Instruments: Methodology, Atmos. Meas. Tech., 8:611–632, 10.5194/amt-8-611-2015, 2015.

Mohan Shankar, Weying Su, Natividad Manalo-Smith, and Norman G. Loeb. Generation of a seamless earth radiation budget climate data record: a new methodology for placing overlapping satellite instruments on the same radiometric scale. Remote Sens., 12 (2787), 10.3390/rs12172787, 2020.

Return to Quality Summary for: SSF Suomi NPP Edition2A